Evaluation by Simulation of an Acoustic Array Composed of Multiple Autonomous Vehicles

by

Kerry Noonan Bosché

B.S., United States Naval Academy (2005)
M.S., Naval Postgraduate School (2006)

Submitted to the Department of Mechanical Engineering
in partial fulfillment of the requirements for the degrees of

Naval Engineer
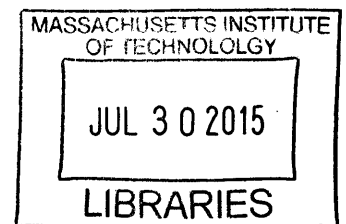
and

Master of Science in Mechanical Engineering

at the

MASSACHUSETTS INSTITUTE OF TECHNOLOGY

June 2015

Signature redacted

Author ..
....

Department of Mechanical Engineering
May 21, 2015

Certified by......**Signature redacted**................

Henrik Schmidt
Professor
Thesis Supervisor

Signature redacted

Accepted by..

David Hardt
Chairman, Department Committee on Graduate Students

Evaluation by Simulation of an Acoustic Array Composed of Multiple Autonomous Vehicles

by

Kerry Noonan Bosché

Abstract

Ship-towed arrays have been integral to Navy combatant operations for many decades. The continual advancement of towed array technology has been continually driven by the need for high sensitivity, low self-noise, and response across a wide range of frequencies. Robotic autonomy, as applied to acoustic sensors, is currently operationally limited to deployment of traditional arrays from semi-submersible tow vehicles. while such a configuration facilitates flexibility in array placement and a measure of stealth, it is an intermediate step toward fully-submerged, autonomous arrays.

In contrast to a traditional hard-wired acoustic array, a "virtual" array, in this thesis, consists of multiple, untethered, hydrophone-equipped autonomous underwater vehicles (AUVs) maintaining alignment by unspecified means. Due to the flexibility of its physical configuration, a virtual array can be both steered in angle and tuned — via element spacing — to optimize response.

This research explores the performance of a simple acoustic underwater virtual array (AUVA). Basic software for controlling an AUVA is implemented and evaluated using computer simulation of array navigation. Simulation of a narrowband, beamforming sonar is used to assess AUVA performance under the control scheme. This research provides a basis for expanding the use of autonomous vehicles for acoustic sensing.

Thesis Supervisor: Henrik Schmidt
Title: Professor

Acknowledgments

THIS PAGE INTENTIONALLY LEFT BLANK

Contents

List of Figures

THIS PAGE INTENTIONALLY LEFT BLANK

Chapter 1

Introduction

1.1 Background

1.1.1 An Abridged History of Towed Array Development

Acoustic arrays have long been an asset to the discipline of undersea sensing. Nearly a century of research and development of arrays and signal processing has yielded a multitude of specialized designs with applications in the fields of research, commerce, and defense. Major advancements in array capability have resulted from the adoption of the latest physical technology, such as array materials and signal processors, or of incorporation of developing knowledge of undersea acoustic propagation.

Among the first practical hydrophone arrays was the *Electric Eel*, a combination towed/hull submarine detection array developed in 1917 by Dr. Harvey Hayes for the US Navy. *Electric Eel*'s geometry facilitated resolution of left/right ambiguity and approximate triangulation of range (see Figure 1-1). A key advantage of Hayes' design was that, for the first time, elements of the array were towed *behind* the ship, where the effect of own ship's noise was much reduced. Operational testing aboard the destroyer USS *Jouett* in early 1918 demonstrated that the array was effective at detecting the submarines of the day [10].

With *Electric Eel* as a jumping-off point, the following array systems are briefly described for historical context and to serve as a prelude to the system evaluated in
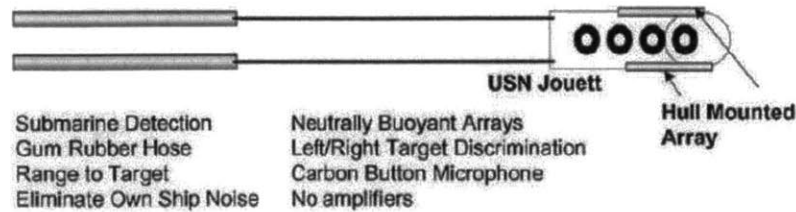
Figure 1-1: The *Electric Eel*, 1917 [10]

this research.

World War II was a relatively dormant period for towed array development, though arrays were built and deployed. The US Navy's *Project General* saw the installation of a towed torpedo detection and destruction array on only 100 of the 2,711 liberty ships built by the Untied States. Notably, none of the array-equipped ships were lost [10, 18]. Several years after Project General — a full 40 years after *Electric Eel* — the beginning of the Cold War would catalyze the next period of towed array development and sustain it into the 1990s.

The first example of the towed array concept that would become ubiquitous for the next several decades was developed in response to the Soviet submarine threat. A series of Navy experiments during the 1950s focused on increasing the reliability and decreasing the self-noise of flexible towed arrays [9]. Operational testing of experimental designs in 1962 led to the development of the AN/BQR-15 towed array, which consisted of a string of hydrophones encased in a flexible, oil-filled hose. The hose was deployed and retracted from a fairing on the exterior of the submarine's hull. The AN/BQR-15 allowed the crews of ballistic missile submarines to detect acoustical energy inside 20-30 degrees of the astern direction (the ship's "baffles"), where physical design and own ship's noise prevented bow-mounted arrays from doing so [10]. From the perspective of hydrophone configuration, the AN/BQR-15 was simpler than *Electric Eel*: though it allowed for detection astern without maneuver, turning was required to resolve left/right bearing ambiguity.

In 1970, to answer the need for anti-submarine surveillance of the Mediterranean, Navy-designed towed arrays returned to surface ships under the Interim Towed Array Sonar System (ITASS) program, and were highly successful [10].

By the late 1970s, commercial towed array "seismic streamer" designs were mature and routinely used for sub-seafloor oil imaging (exploration seismology). The superior low-frequency response of these arrays suited them to long-range ocean surveillance, a fact recognized by the Navy. In 1982, Whitehall Industries won a contract to provide a seismic-type array for the Surveillance Towed Array Sonar System (SURTASS) [11].

From the 1960s into the 1990s, advances in ship and submarine silencing motivated improvements in towed array design and signal processing. While the basic form of military towed arrays has changed little since the beginning of the Cold War, modern designs take advantage of key technological advances. Improvements in array construction have facilitated longer arrays, while the introduction of high-data-rate fiber-optic hydrophones and cabling in the 1990s functionally removed the limit on the number of sensor channels. Both of these advances drove improvements in bearing resolution and low-frequency response.

1.1.2 Acoustic Array Configurations

The following descriptions provide a context for subsequent discussion of virtual array geometry.

Horizontal Line Array

For practical reasons, the most common towed array design in military use is the horizontal line array. Though systems vary, a typical array consists of a number of hydrophones encased in a flexible, oil-filled tube. The length of the array is largely a function of desired frequency response; low-frequency surveillance arrays such as SURTASS can be 1,500 meters long, and seismic streamers can reach up to 10 kilometers [17]. Arrays carried by warships, which are designed for compact onboard storage and higher frequency response, are typically less than 1,000 meters in length [16]. While towing behind a ship naturally tends to maintain a horizontal line array near its intended configuration, precise array geometry is seldom perfectly linear due to maneuvering and aft-end "droop." Some modern array systems use processing

corrections to account for these geometry perturbations to some degree. The main limitation of a many horizontal line arrays, when towed alone, is bearing ambiguity: in simple form, line array beamforming can only discern signal bearing relative to the array heading, with each "beam" corresponding to a conical surface centered on the array axis. For surface targets, this translates to left/right bearing ambiguity. For submerged targets, especially at relatively close range, target bearing and azimuth can be confounded, complicating target motion analysis. It should be noted that there is a solid theoretical basis for left/right ambiguity resolution by exploiting, if known, the perturbations of a linear array [6, 4]. Such capability necessarily requires additional processing resources.

A straightforward solution to the bearing ambiguity problem is deployment of multiple towed arrays. With complementary signal processing, the result is, by definition, a parametric array. To acquire the high-resolution three-dimensional images required for oil exploration, six to eight (and occasionally up to 12) seismic streamers are commonly towed [15]. Military vessels which carry both high- and low-frequency arrays may tow both simultaneously — thought independently, without the processing to resolve ambiguity — in order to monitor a wider frequency range.

Vertical Line Array

A vertical array is in many ways identical to a horizontal array. Vertical arrays are often ideal for applications in which a stationary array is desired, due to the impracticalities of maintaining a straight vertical shape in a long, flexible array while towing. Under a simple beamforming scheme, the conical beams formed by a vertical array lead not only to confounding of range and bearing, but to complete 360-degree bearing ambiguity. In the context of matched-field processing, discussed below, the key advantage of a vertical array lies in its ability to discern variations in acoustical energy along the water column. Coupled with more complete knowledge of the local sound speed profile (SSP), this facilitates source range/depth localization to a higher degree of accuracy. Permanent and expendable synthetic-aperture vertical arrays, consisting of a single hydrophone moved vertically in the water column, have been

evaluated [14, 12].

Parametric Array

The most recognizable parametric arrays are bow-mounted spherical or conformal designs on military combatants. Due to relatively complicated geometry, parametric arrays are not easily towed or externally stored. For this reason, towed parametric arrays are not common outside of the geophysical industry. The application of autonomous underwater vehicles (AUVs) to parametric array designs is discussed in subsequent chapters in the context of virtual arrays.

1.1.3   Signal Processing

A general introduction to two broad approaches to sonar signal processing is provided for context.

Plane Wave Beamforming

Plane wave beamforming is ubiquitous as the historical basis of sonar signal processing. Using known properties of sound propagation through water, the array-geometry-dependent signal arrival delays can be calculated for each direction of arrival. For a one-dimensional (line) array, the direction is defined in one dimension (e.g. degrees relative to the array axis). For parametric arrays in two and three dimensions, localization is possible in two dimensions (e.g. azimuth and elevation). Because the incoming wave is generalized to that of an infinitely distant source, resulting in a planar rather than spherical wave front, plane wave beamforming precludes range estimation without the addition of other techniques.

Matched-Field Processing

In the absence of geographic-scale obstacles, the propagation path of an undersea acoustic signal is determined largely by the local sound speed profile (SSP) via refraction, and the topography of the sea floor (reflection and absorption). Consequently,

the particulars of a propagation pattern are largely a function of depth.

If the propagation of a wavefront were to be observed from above, it would expand roughly in the shape of a circle. If observed along the signal-to-array axis, however, the wavefront would be seen to distort as a function of the local SSP. Traces perpendicular to the wavefront, representing the path of energy through the water, take curved paths; the degree of curvature depending on the slope of the SSP.

When applied to a horizontal line array, the conical beam of a plane wave beam-former cuts vertically through the water column; localization is therefore only a bearing. Because of the uniformity of acoustic propagation in the horizontal plane, horizontal line array data is generally processed without SSP data. Range estimation is accomplished using other methods such as signal strength analysis, ranging maneuvers, or propagation modeling.

If the local SSP is known through historical or in-situ bathymetry, the signal strength of for any source on the range-depth plane can be quantified. This signal strength field serves as a prediction for the signal strength at the array. In matched-field processing (MFP), the received signal is compared to the expected signal for any number of two-dimensional source locations. If directionality can be exploited using directional sensors or multiple arrays, source bearing, range, and depth can be estimated [8].

MFP can be applied to any array geometry, but arrays which exploit vertical variation in signal strength are particularly suited. A vertical line array is the simplest of these designs.

1.2 Motivation

The US Navy recognizes AUVs as a rapidly-maturing technology that can be utilized in a broad range of missions, including undersea surveillance [5]. Though proven mission- and payload-flexible platforms such as Bluefin Robotics' *Bluefin-21* and derivative Navy systems under development represent prototypes for fully-submersible autonomous operations, there are many applications left to explore. As applied to

acoustic arrays, the first application of AUVs is sensor towing. Decoupling an acoustic sensor from the mother platform allows both ship and sensor increased operational flexibility and stealth. The semi-submersible Remote Multi-Mission Vehicle (RMMV) towing the AN/AQS-20 mine-detecting sonar is an operational example of this configuration. For the forseeable future, the size and aperture of an array towed from an AUV is limited by towing power.

A possible next step in autonomous underwater sensing is the deployment of one or more hydrophones on multiple AUVs to form an autonomous underwater "virtual" array (AUVA). As an alternative to AUV-towed arrays, an AUVA could potentially maintain a relatively large aperture and exploit adaptable geometry based on target or environmental characteristics.

This thesis explores some high-level aspects of the control and performance of a simple AUVA to establish a baseline for feasibility and performance. In the interest of immediate relevance, the assumptions and methods of this analysis apply to a prototype system that could be assembled in an academic setting in the near future, without excessive integration effort.

1.3 Outline

This document is organized into six chapters:

1. Chapter 1 establishes the motivation of this research by summarizing the relevant history of towed arrays, and introducing relevant topics in signal processing.

2. Chapter 2 describes the array system to be evaluated, including notional hardware selection and basic concept of operations. Selected aspects of the system which affect sensing performance are identified for evaluation.

3. Chapter 3 contains heuristic and quantitative analyses of AUVA performance based on array geometry.

4. Chapter 4 describes a how a simulation of an AUVA was implemented.

5. Chapter 5 summarizes the design and results of multiple AUVA mission simulations.

6. Chapter 6 outlines the findings of this research and suggest areas for further study.

Chapter 2

The Array

2.1 Description
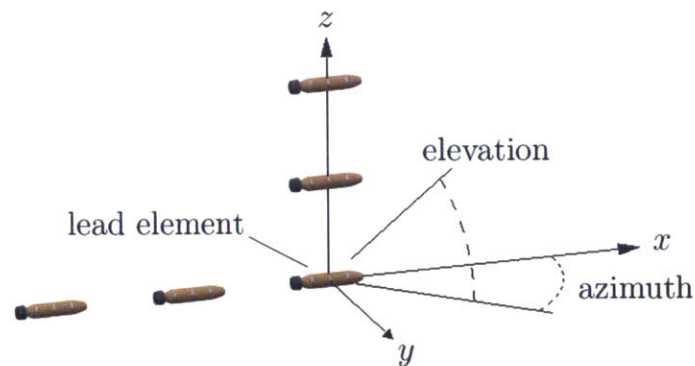
Figure 2-1: L-Shaped AUVA and coordinate plane

Physical Description

An AUVA is defined in this thesis as an array whose sensor elements are distributed among two or more AUVs. Alternatively, an AUVA comprises multiple AUVs — the array *elements* — each carrying one or more sensors. Sensors may be integrated into the vehicle, attached externally, or towed. As the primary strength of an AUVA is the distribution of elements *across* vehicles, the specifics of sensor-vehicle integration are not addressed.

19

Vehicles
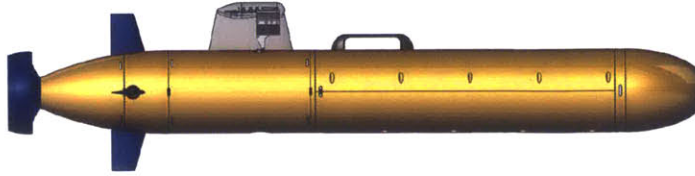
Figure 2-2: *SandShark* AUV (Courtesy of Bluefin Robotics)

The elements that make up the AUVA are not specified apart from the capabilities defined below. Commercially available platforms such as Bluefin Robotics' *SandShark* are mission-flexible by design, compact, and would be ideal for principal investigation into an AUVA. Mature AUVA designs, however, would likely take advantage of the size and weight efficiencies of a purpose-built design. Smaller vehicles would also allow for greater operational flexibility, as tighter array geometries increase the likelihood of physical interference of vehicles.

Equipment

For the sake of generality, no specific array equipment is prescribed. At a minimum, however, AUVA elements would be capable of:

- Autonomy of navigation for deployment from and return to mother ship as well as maintenance of array geometry.

- Submerged positioning (for the lead element, at a minimum) via inertial navigation (INS) or an equivalent system.

- Surfaced positioning, for individual element backup or deployment/return.

- Inter-vehicle positioning for maintaining array geometry.

- Temporary storage of received signals, including accurate timekeeping synchronized across all elements.

- Surfaced over-the-air transmission of recorded signals to the mother ship.

The relative difficulty and bandwidth limitations of underwater data transmission preclude its meaningful application in the case of a simple, prototype AUVA. The immediate consequence of this exclusion is that it eliminates the capability for autonomous array adaptation to the composite acoustic picture.

The relatively low positional accuracy of AUV-deployable INS systems is non-trivial. However, multiple mitigating factors support its omission from consideration in an initial investigation of an AUVA:

- The primary purpose of an array track, whether preplanned or adaptive, is to maneuver the target in bearing relative to the array. The specific shape and position of the array track is a secondary consideration (for non-synthetic apertures, forward motion is in fact only necessary for creating the hydrodynamic forces required for maneuvering).

- For typical detection ranges of thousands of yards, and with sufficiently accurate recording of lead element heading, the entirety of an array's path over a data collection cycle can be reasonably reduced to a point without significant loss in target true bearing accuracy.

2.2 Concept of Operations

The following sequence describes a notional AUVA mission, with attention given to the constraints of existing, reasonably-obtainable equipment. It is recognized that one could defend countless variations to this concept. However, with the exception of the lead-element navigation scheme, the specifics do not bear heavily on the conclusions of the analysis.

Preparation

Array elements are prepared for submerged operations. Mission parameters, such as lead element track, target parameters, mission duration, contingency behaviors, etc. are transmitted to the vehicles by wired or over-the-air connection.

Deployment

Array elements are individually placed in the water from one or more motherships and submerge to achieve and maintain the desired array geometry. A future virtual array system would likely include equipment facilitating the simultaneous deployment of several elements, but such capability does not affect the conclusions of this analysis.

Submerged Data Collection

While collecting and storing received signals, each element uses inter-vehicle positioning to maintain its prescribed position relative to the lead element. With the aid of a submerged navigation system, the lead element drives a preprogrammed track in the form of waypoints or a similar behavior. A collection phase may end at a preprogrammed cue or upon a recall signal.

Data Transmission and Processing

The array elements surface and transmit data over-the-air to a receiving platform. Alternatively, and for development purposes, data may also be downloaded from vehicles after recovery. Array data is processed by any number of means and/or stored for later processing.

2.3   Issues for Analysis

For the purpose of comparison, modern tactical and surveillance towed array systems have the following attributes:

- Relative hydrophone positions are correlated and may be known to a high degree of accuracy. Additionally, when array geometry is non-ideal due to speed-dependent-droop or during a maneuver, corrections based on experimentation can be applied during processing.

- Signals are processed and interpreted in near-real time.

- The number of hydrophones is primarily limited by processing power (hydrophone count for a modern towed array is typically in the hundreds).

- Array aperture is limited by the towing and storage capability of the towing platform.

In contrast, for the AUVA described above:

- Relative geometry may be uncorrelated and, unless recorded from the inter-vehicle positioning system, unknown.

- Signals are recorded and transmitted for processing after a data collection period.

- Vehicle cost and the logistics of multi-vehicle deployment place practical limits on the number and density of hydrophones.

- Array aperture is limited by the capability (effective range) of the inter-vehicle positioning system.

A "worst case" scenario for AUVA performance would ignore non-ideal array geometry in processing and place practical limits on the number of elements and their spacing, limiting aperture.

2.4 Array Geometry

The geometry (relative position of elements; "shape") of an AUVA is expected to have a significant effect on localization performance (see Chapter 3). An L-shaped array was chosen for consideration in this research for several reasons:

- If only omni-directional hydrophones are considered, one-dimensional arrays — vertical or horizontal — are limited to localization in one dimension: bearing relative to the array axis.

- A two-dimensional array consisting of more than two linear segments is anticipated to exhaust limited vehicle resources without a justifiable improvement in overall resolution. Two orthogonal segments is anticipated to be an acceptable compromise. This suggests a cross-shaped array with identical, intersecting segments.

- It is anticipated, given the leader-follower scheme outlined in section 2.2, that placing a follower vehicle *ahead* of a leader vehicle will lead to undesired difficulty in array alignment programming.

An L-shaped array (Figure 2-1), with the lead vehicle at the intersection of the vertical and horizontal segments, addresses these concerns. A more thorough comparative analysis of array geometries is suggested in Chapter 6.

Chapter 3

Array Geometry and Performance

3.1 The Cramér-Rao bound

It is useful to quantitatively predict performance of an array as part of the design process. Namely, the accuracy of bearing estimates is of concern. A common approach is to calculate the mean squared error of the bearing estimates. In general, and especially in cases where an estimator is not identified, it can be simpler to calculate a lower bound on the variance of *any* estimator. One such method with established use in acoustic literature is the Cramér-Rao bound (CRB) [2, 7].

The CRB states that the inverse of the Fisher information of an unbiased estimator is the lower bound of its variance. In the case of an AUVA, the parameter to be estimated is a source angle θ by estimator $\hat{\theta}$ (azimuth and elevation bounds are calculated seperately).

In this analysis, calculation of the CRB begins with finding the cross-spectral density matrix $\mathbf{K}(\mathbf{a})$ for a given array-target geometry $\mathbf{a}$, defined by the array element positions (based on the chosen array shape) and the target's azimuth and elevation relative to the reference element. $\mathbf{K}$ is the sum of the cross-spectral densities of the

signal and uncorrelated noise.

$$\mathbf{K} = \mathbf{K}_s + \mathbf{K}_n = \hat{\mathbf{w}}^\dagger \mathbf{S} \hat{\mathbf{w}} + \mathbf{K_n} \tag{3.1}$$

$$= \begin{bmatrix} \hat{w}_0 \\ \vdots \\ \vdots \\ \hat{w}_N \end{bmatrix} \begin{bmatrix} 1 & 0 & \cdots & 0 \\ 0 & 1 & \cdots & 0 \\ \vdots & \vdots & \ddots & \vdots \\ 0 & 0 & \cdots & 1 \end{bmatrix} \begin{bmatrix} \hat{w}_0 & \cdots & \cdots & \hat{w}_N \end{bmatrix} + \frac{1}{\text{SNR}} \begin{bmatrix} 1 & 0 & \cdots & 0 \\ 0 & 1 & \cdots & 0 \\ \vdots & \vdots & \ddots & \vdots \\ 0 & 0 & \cdots & 1 \end{bmatrix} \tag{3.2}$$

$$= \begin{bmatrix} \hat{w}_0 \\ \vdots \\ \vdots \\ \hat{w}_N \end{bmatrix} \begin{bmatrix} \hat{w}_0 & \cdots & \cdots & \hat{w}_N \end{bmatrix} + \frac{1}{\text{SNR}} \begin{bmatrix} 1 & 0 & \cdots & 0 \\ 0 & 1 & \cdots & 0 \\ \vdots & \vdots & \ddots & \vdots \\ 0 & 0 & \cdots & 1 \end{bmatrix} \tag{3.3}$$

In the expressions above, $\hat{\mathbf{w}}$, a function of array-target geometry and target frequency, is a complex *steering vector* of phase corrections. The cross-spectral density of noise $\mathbf{K}_n$ is dependent on the signal-to-noise power ratio (SNR), and indicates uncorrelated element noise.

The elements of $\mathbf{J}$, the Fisher information matrix $\mathbf{K}$ are given by

$$J_{ij} = \text{Tr}\left[\mathbf{K}^{-1}(\mathbf{a}) \frac{\partial \mathbf{K}(\mathbf{a})}{\partial a_i} \mathbf{K}^{-1}(\mathbf{a}) \frac{\partial \mathbf{K}(\mathbf{a})}{\partial a_j} \right] \tag{3.4}$$

Where azimuth and elevation angles are treated separately, the Fisher information can be expressed as a univariate function of θ.

$$J = \text{Tr}\left[\mathbf{K}^{-1}(\mathbf{a}) \frac{\partial \mathbf{K}(\mathbf{a})}{\partial \theta} \mathbf{K}^{-1}(\mathbf{a}) \frac{\partial \mathbf{K}(\mathbf{a})}{\partial \theta} \right] \tag{3.5}$$

In this case, the Cramér-Rao bound is stated formally as an inequality.

$$\sigma_\theta^2 \geq J^{-1} \tag{3.6}$$

3.2 Comparative Results

To facilitate comparison, the two-dimensional CRB surfaces of multiple reference arrays are included here. The first is a vertical line array comprising nine elements spaced three meters apart. It is important to note that the steering vector $\hat{\mathbf{w}}$ in the formulation above is frequency dependent. The CRB response below corresponds to a 220 Hz source ($d/\lambda = .44$).

| (a) Azimuth | (b) Elevation | (c) Azimuth minus elevation |
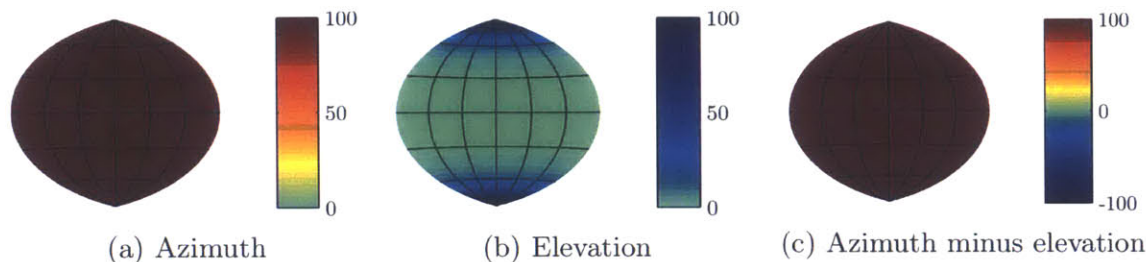
Figure 3-1: CRBs for 9-element vertical array; 220 Hz source (d/λ=.44); SNR=5.

Each plot in Figure 3-1 is a Hammer projection of the possible source locations in the array's right (positive y-axis) hemisphere (see Figure 2-1). The horizontal axis represents 0-180° relative to the array heading; elevation angles -90° to 90° are on the vertical. Figure 3-1a, the CRB response for azimuth angle, is infinite at all points as a vertical line array cannot discern horizontal angle of arrival. Note that the color scaling is limited to the interval $[0, 100]$ for clarity. The elevation response, Figure 3-1b, illustrates the characteristics of plane-wave beamforming for a linear array: the CRB is smallest for elevation angles near zero (on the "beam" of the array), and asymptotically approaches positive infinity at either vertical extreme (array "endfire"). The third plot, Figure 3-1c, is a composite CRB, formulated as $\text{CRB}_{azimuth} - \text{CRB}_{elevation}$. For this array, the composite CRB is dominated by the azimuth CRB, and is not instructive.

The second comparison array also comprises nine elements, but has the shape of a swiss cross: it has a 5-element vertical and horizontal sections (the center element is shared). Not surprisingly, the horizontal section facilitates azimuth resolution (finite CRBs in Figure 3-2a). The elevation CRB response (Figure 3-2b) is similar to the vertical array, but greater at all points due to fewer vertical elements. It is im-

27

(a) Azimuth   (b) Elevation   (c) Azimuth minus elevation
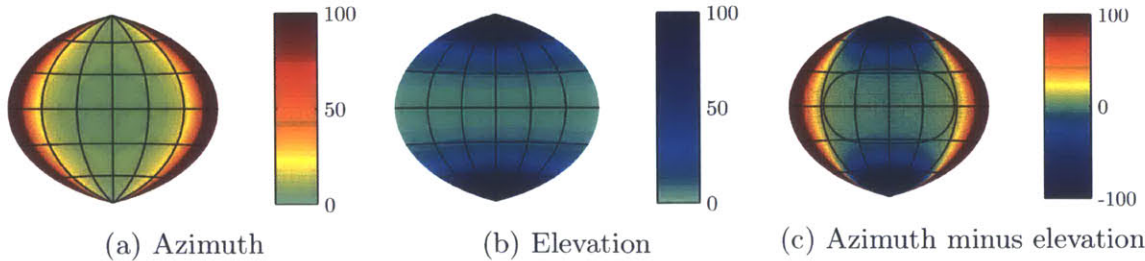
Figure 3-2: CRBs for 9-element cross-shaped array; 220 Hz source (d/λ=.44); SNR=5.

portant to note while interpreting the plots that although the cross-shaped array is rotationally symmetric and both array segments have identical properties, they are not symmetric with respect to the coordinate system. Constant azimuth surfaces are planar while constant elevation surfaces are conical.

Figure 3-2c demonstrates that a cross-shaped array can be expected to perform relatively poorly for sources that are near the plane of the array. In the vertical poles, high CRBs are dominated by elevation response; ahead and behind the array (near 0° or 180° azimuth), azimuth response dominates. The contour in the figure bounds the region in which $\mathrm{CRB}_{azimuth} + \mathrm{CRB}_{elevation} \leq 10$. Intuitively, this region is centered on the beam of both array segments.

(a) Azimuth   (b) Elevation   (c) Azimuth minus elevation
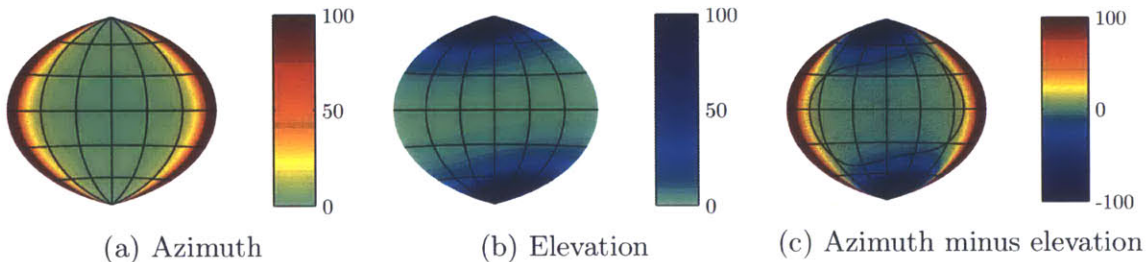
Figure 3-3: CRBs for 9-element L-shaped array; 220 Hz source (d/λ=.44); SNR=5.

The CRB response shown in Figure 3-3 is that of a nine-element, L-shaped array (see Figure 2-1); element spacing is identical to the previous. The response is nearly identical to that of its cross-shaped counterpart with the exception that the asymptotic behavior of the elevation CRB is slightly rotated about the array's y-axis: toward the front of the array (0° azimuth) at high elevation angles, toward the back of the array at low elevation angles. The composite CRB response (Figure 3-3c) is similar in form to that of the cross-shaped array, and is affected by the same shift.

28

Notably, the region of low CRBs enclosed by the contour is not only shifted, but larger.

(a) Azimuth (b) Elevation (c) Azimuth minus elevation
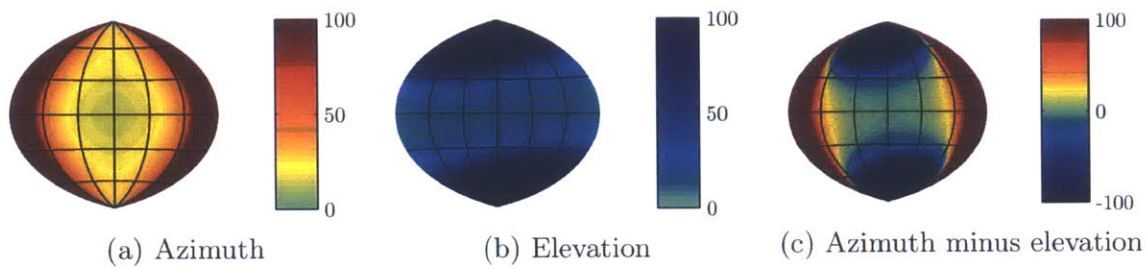
Figure 3-4: CRBs for 5-element L-shaped array; 220 Hz source (d/λ=.44); SNR=5.

Figure 3-4 is the CRB response of the AUVA geometry evaluated in the following chapters. It is identical to the previous example, but with only three elements in each segment (five elements total). While the CRB is significantly greater at all points, the basic structure of the response is the same. There is no region in which the summed CRBs are less than ten.

THIS PAGE INTENTIONALLY LEFT BLANK

Chapter 4

Array Simulation Methods

4.1 Simulation Code Architecture

The physical simulation of the AUVA was implemented using an open-source code architecture called MOOS-IvP.

4.1.1 MOOS
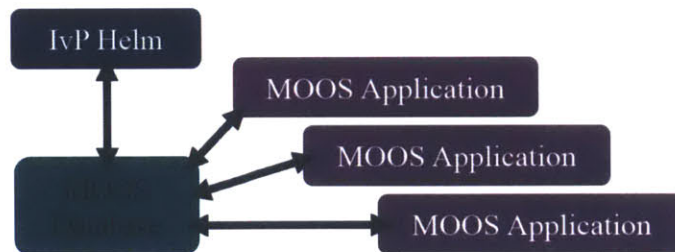
Figure 4-1: Basic MOOS-IvP Code Architecture

MOOS (Mission-Oriented Operating Suite) was developed in 2001 to support marine robotics research at MIT. At its core, an implementation of MOOS consists of a database of shared information and several applications that publish to and/or subscribe from that database, collectively referred to as a MOOS *community*. The MOOS architecture is highly modular in that applications can be added, removed, and upgraded as needed. A host of useful applications are available along with the MOOS package, as are tools to create new ones [1, 3].

MOOS applications provide a wide variety of functions for an autonomous vehicle. For example, applications are generally used to:

- Provide an interface between sensors (sonar, GPS, bathymetric sensors, etc.) and the database.

- Facilitate communication between MOOS communities running on separate vehicles or shore-based nodes.

- Support logic to inform navigation decision making.

4.1.2 IvP

The IvP (Interval Programming) Helm ("the helm") is a MOOS application developed at MIT in 2004 to support vehicle autonomy. The helm facilitates the management of multiple vehicle objectives using a form of optimization. Vehicle objectives are coded in *behaviors*, each of which provides a *helm function* — an encoding of the "goodness" of possible course, speed, and depth combinations — to the helm. The helm reconciles these to provide a best-overall navigation input to the vehicle [3, 1].

A simple example of the utility of the IvP Helm would be an autonomous survey vehicle that must follow a predetermined track to the extent possible, but which must also avoid collision with other vehicles. In the same way a human pilot would, the helm behaviors can prioritize the survey when collision avoidance maneuvers are not necessary (when other vehicles are distant or not detected), but leave the survey track as necessary to avoid collision.

4.1.3 Mission and Vehicle Configuration

In the MOOS-IvP architecture, a *mission* — the deployment of a vehicle to complete one or more objectives — is configured using a *mission file*. The mission file specifies the applications that will run alongside the database and the helm, and provides an interface for application configuration.

Vehicle behaviors are called and configured using a *behavior file*, whose function is analogous to that of the mission file. MOOS-IvP provides tools that allow variables within mission and behavior files to be set from the command line. This allows for straightforward manipulation of mission and vehicle parameters as well as semi-automated configuration of multiple vehicles. MOOS-IvP missions are generally initiated by executing a shell script with one or more arguments, which may in turn call other scripts. In the case of the AUVA, a top-level launch script accepts as arguments basic AUVA parameters, such as number of elements, element spacing, and array depth, and individually configures each vehicle community using a *for* loop.

4.1.4   Mission Simulation with MOOS-IvP

Typically, each vehicle or shore-based node hosts its own community. Pertinent data is shared between the communities' databases to facilitate reporting, aggregation, or cooperative behavior. In simulation, however, the communities involved in a mission can be run on a single machine or on a set of networked machines.

The public MOOS-IvP distribution includes two critical simulation tools, *pMarineSim* and *pMarineViewer*. The first uses hydrodynamic principles and vehicle properties to simulate the motion of surfaced and submerged vehicles through the water. The second provides a graphical user interface including a live map view of actual or simulated vehicles. MOOS-IvP also includes tools for logging and playback of vehicle telemetry.

4.2   The AUVA Mission

The functionality of the AUVA mission is spread across multiple on-vehicle communities and one non-vehicle "shoreside" community.

This section refers only to the simulation of the vehicles' motion through water. Sonar processing is simulated separately and will be discussed below.

Mission Overview

The simulated AUVA in this analysis comprises a *lead element*, which is responsible for driving preprogrammed waypoints, and *follower elements*, whose sole navigational task is to maintain their prescribed position with respect to the leader.

4.2.1 On-Vehicle MOOS Communities

All vehicle communities in the AUVA are launched with identical mission and behavior files. By configuration, however, one vehicle performs the functions as the lead element while the others follow. Both leader and follower functions are controlled by a small number of applications and behaviors. Those critical to the operation of the array are described here.

- *BHV_Waypoint* is a standard behavior included in the MOOS-IvP distribution. The behavior directs the vehicle to navigate through an ordered set of waypoints defined in the behavior file, and can be configured to repeat upon completion. In the AUVA mission, waypoint behavior is only called for the lead element (element number one).

- *pLeadElement* is an application created for the AUVA, and serves as a communication interface between the vehicles. In the lead element community, the application regularly pulls the vehicle's telemetry, including a time stamp, from the local database and arranges it into an unencoded, delimited string. This string is published to the local database as a message, from where it is redistributed to the other vehicles (by standard MOOS applications not described here). In follower element communities, the received message is parsed and the lead element telemetry values are published to the database to be used by the *BHV_L_Element_Follow* behavior described below.

- *BHV_L_Element_Follow* is a behavior written for AUVA simulation. The behavior subscribes to the lead element telemetry in the local database. On each iteration, the time-stamped lead element telemetry is used to calculate the

34

dead reckoning (DR) position of the lead element. Depending on the follower element's element number, its ideal position is a simple offset from the lead element's DR position. To minimize *searching* (oscillation of the follower path on either side of the lead element path), the behavior calculates a *rendezvous point*, the lead element's predicted position a fixed amount of time (the *lead time*) in the future. The follower element's offset is applied to the lead element rendezvous point; the resulting point in space is the "goal" point for that iteration. The behavior returns a helm function which prioritizes the course and speed combination that would achieve that point in exactly the lead time (due to continual recalculation, the point is never achieved). For all vehicles, *BHV_L_Element_Follow* has the collateral function of logging telemetry data to a comma-delimited text file to be used by the sonar simulation.

Other "stock" behaviors are active on the vehicles, including those that maintain vehicle depth, define an operating region, and allow for station keeping. None of these affect the operation of the AUVA as it applies to this research.

4.2.2   Shoreside MOOS Community

This simulation applies basic MOOS functionality in a way that requires an off-vehicle community to process inter-vehicle communication and facilitate simulation monitoring. This community is an artificiality; it does not perform a command and control function as a mothership would for array deployment. Similarly, the mothership does not facilitate inter-vehicle communication under this AUVA concept of operations, as each element navigates independently off of the lead element.

The critical off-vehicle functions are performed by these MOOS applications:

- The standard MOOS applications *pShare* and *uFldNodeComms* facilitate refereed communication between vehicles. *pShare* provides the basic functionality, while *uFldNodeComms* allows for constraints on message length, minimum interval between messages, communications ranges, etc.

- *pMarine Viewer*, mentioned previously, is a graphical user interface featuring a real-time map view of vehicles and several tools for interacting with running MOOS communities.

4.3   Plane-Wave Beamforming

The basic sensing performance of the AUVA was investigated by implementing a simple plane-wave beamformer in MATLAB. This section describes important aspects of the sonar simulation in the approximate order of their implementation.

4.3.1   MOOS-IvP/Sonar Simulation Interface

Since the AUVA here is not required to maneuver adaptively, the physical and sonar simulations of the AUVA need not be coupled in real time. The source/element geometry input necessary for the sonar simulation comes in part from the physical simulation, during which *BHV_L_Element_Follow* writes selected vehicle telemetry data to a common file. The log file is processed by the MATLAB script *read_array_log.m*, which uses cubic splines to smooth the data from all vehicles and interpolate onto a common time series. Source location is manually specified by the user while configuring the sonar simulation. This decoupled approach allows multiple acoustic scenarios to be simulated against the same array time-series geometry.

4.3.2   Simulation Configuration

The sonar simulation is configured by defining the *scenario* data structure, including:

- *scenario.array*. The ideal array geometry defined by an N-by-3 array, where each row is the displacement in meters of each of N elements from the lead element.

- *scenario.array_data*. The interpolated array telemetry data described in Section 4.3.1.

- *scenario.source* defines the location, depth, and frequency of the source.

- *scenario.SNR* defines the signal-to-noise power ratio at each element.

4.3.3 *Bellhop* Interface

Bellhop is an acoustic beam-tracing software suite that allows calculation of transmission loss, arrival characteristics, eigenrays, and time-series arrivals [13]. Originally coded in Fortran, *Bellhop* is freely available in a variety of formats, including a collection of MATLAB scripts that either serve the same functions as the original programs or provide a familiar means to interact with them. In this simulation, *beamformer.m* (described in Section 4.3.4) and supporting scripts utilize *Bellhop* to calculate the complex signal amplitude at each element for each time step.

1. Array and source geometry from *scenario.array_data* and *scenario.source* are compared to produce an array of all possible element range/depth displacement combinations from the source, to one-meter precision.

2. A pre-formatted *Bellhop* configuration file is modified to include the element range/depth combinations, source frequency, and source depth. The file also defines the sound speed profile (SSP).

3. *Bellhop* is called, producing a file containing structured list of arrivals at each range/depth point. The arrival amplitude, total propagation delay, and receiver angle are used by *beamformer.m*. The source angle and numbers of top and bottom reflections are also provided for each arrival. The arrivals file is parsed and stored as a data structure.

4. At each time step and for each element, the physically closest range/depth combination is found. A plane-wave phase correction is applied to the arrivals based on the element's offset from the reference point, and the arrivals are summed. At this step, attenuation can be ignored by correcting the lead amplitude to $1 + 0i$ (the source amplitude) and applying the same correction factor to the other element signals.

37

4.3.4 *beamformer.m*

beamformer.m is the top-level sonar simulation script, and requires as input the *scenario* data structure and the *Bellhop* environment template.

Sonar functionality is simulated in time-series — a complete "picture" is produced for each second of array simulation — but not in real time. At each time step, the complex signal amplitude is calculated, accounting for multi-path arrivals and a specified SSP (see Section 4.3.3). For each azimuth/elevation combination, a beamforming or *replica* factor is applied to the element signals based on *ideal* array geometry. The summed signal is the array response for that direction and time.

At each time step, *beamformer.m* stores the current sonar "picture," the array gain (dB) for all azimuth/elevation combinations, assuming unit source strength. An average response is also calculated. The current and overall direction of maximum response are identified and recorded.

The script returns a *simulation* data structure including the information above as well as some plot configuration data. The original *scenario* data structure is also appended to *simulation*.

4.3.5 Plotting

A separate script uses the *simulation* data structure to plot the sonar results. At each time step, *plot_beamformer.m* plots the current and average array response surface. Markers showing the maximum response and actual source direction are also plotted. These plots allow visual identification of strong response areas as the sonar picture evolves. The azimuth axes of both plots are plotted as true bearing (clockwise from North) by correcting for the lead element heading. An example plot is displayed as Figure 4-2.
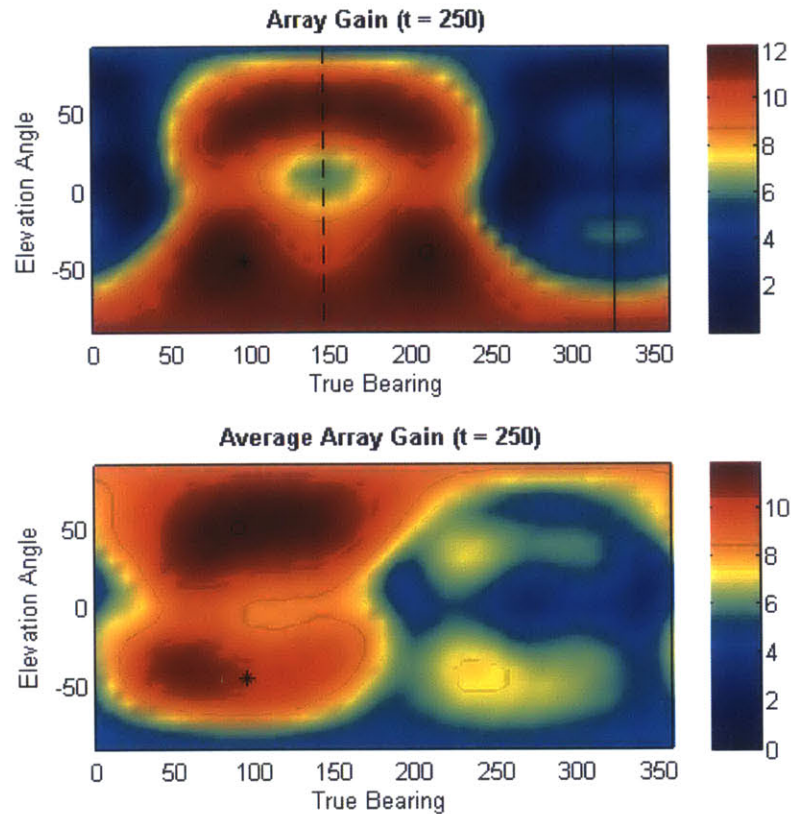
Figure 4-2: Example Array Response MATLAB Output

The sonar picture above is from 250 seconds into a simulation. The array has maneuvered to a heading of approximately 330° and is currently in near-ideal geometry. The current regions of maximum response (top) are in the vicinity of the true target direction (marked by an asterisk) of 090°, -45° elevation, and in an upper elevation due to surface reflection. The reponse is mirrored on the opposite side of the astern direction (dashed vertical line) due to bearing ambiguity. The overall response (bottom) shows that left/right bearing ambiguity has been resolved by maneuver. In both plots, the experimental maximum return is marked with a circle.

THIS PAGE INTENTIONALLY LEFT BLANK

Chapter 5

Mission Design and Results

5.1 Mission Design

Several AUVA missions were conceived with the objective of capturing major source localization performance factors. Each of the the eight primary missions share several characteristics:

- An AUVA comprising five vehicles (three vertical and three horizontal elements); this is considered to provide satisfactory localization performance while representing a manageable number of small AUVs for eventual in-water testing.

- A lead element speed of 1 m/s (1.94 knots), which provides margin over steerageway for maneuvering without contributing to excess misalignment times.

- A total track distance of 600 meters, requiring approximately 10 minutes for completion. This is considered to be a reasonably short period of time in between sonar "picture" updates under any surveillance and most tactical scenarios. It is also performance-limiting from a mission perspective, and provides a baseline for comparison. Modifying an AUVA mission for longer duration is straightforward, and would necessarily lead to better results.

The primary missions differ only in the geometry of their waypoints. Each successive mission is designed to align the array on a larger number of distinct headings,

41

at the anticipated cost of alignment: the more the array turns during the mission period, the less time the array spends in near-optimal alignment on any of its mission legs. The primary AUVA missions are listed here:

1. Picket ("back and forth"), 150-meter legs.

2. Picket, 300-meter legs.

3. Triangle, 200-meter legs.

4. Square, 150-meter legs.

5. Pentagon, 120-meter legs.

6. Hexagon, 100-meter legs.

7. Heptagon, 86-meter legs.

8. Octagon, 75-meter legs.

5.2   Simulation Results

5.2.1   AUVA Maneuvering Phenomena

Discreet Turns

By design, AUVA follower elements do not anticipate maneuvers. Consequently, as in a traditional towed array, a turn is followed by a period of instability whose characteristics vary with the magnitude of the turn. Figure 5-1 illustrates array geometry throughout a 90° turn. Immediately prior to the turn, array geometry is ideal. The turn is initiated by the lead element's waypoint behavior, and for a short period only the lead element has maneuvered (5-1b). In time, the follower elements begin to turn in response. It is important to note that although the follower elements maintain approximate linearity throughout the misaligned period, their axis is not parallel to the lead element heading (5-1c through 5-1e). This is a source of systematic bearing error during turns, as the array heading is assumed to match that

of the lead element. Finally, as the array approaches realignment (5-1f through 5-1h), some overshoot again contributes to bearing error.

(a) Pre-turn (t = 0 s)   (b) t = 9 s   (c) t = 18 s   (d) t = 27 s

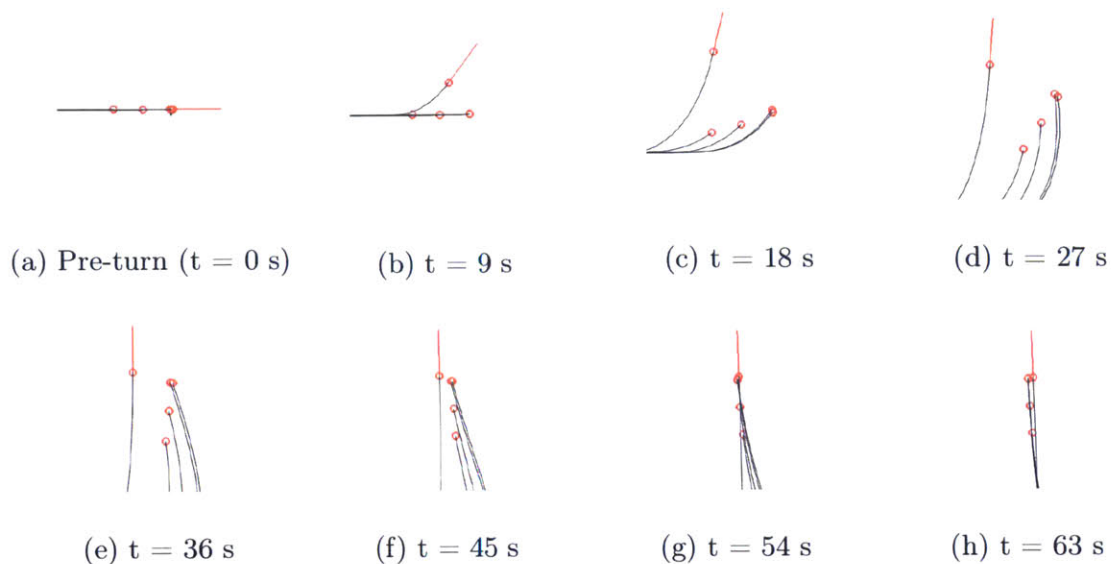(e) t = 36 s   (f) t = 45 s   (g) t = 54 s   (h) t = 63 s

Figure 5-1: Element Paths During a 90° Turn

No single, meaningful criteria for establishing array alignment vs. misalignment is apparent from this analysis, but a general comparison of ideal vs. actual array geometry yields predictable results. Figure 5-2 summarizes the following discussion.
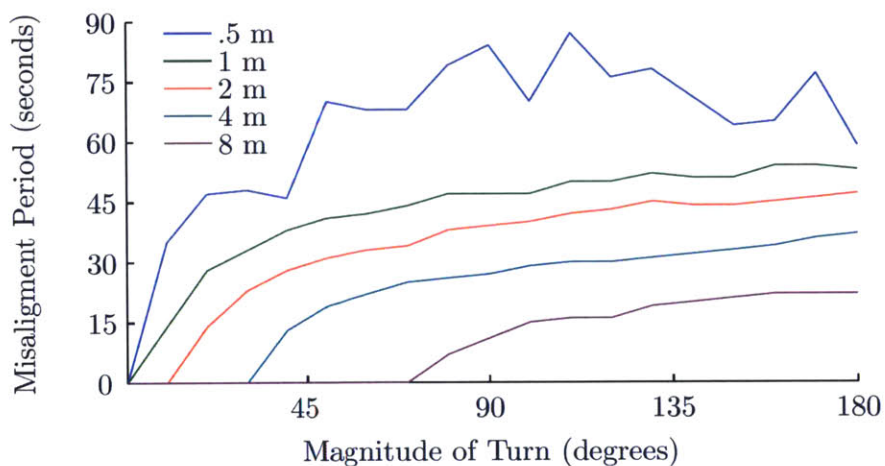

Figure 5-2: AUVA Turn Misalignment Time for Varying Alignment Thresholds

In order quantify the effect of maneuvering in alignment, a series of turns, from 10° to 180°, were first simulated as separate missions. At each time step, the array

43

was determined to be aligned if *all* follower elements were within a threshold distance of their ideal position with respect to the lead element. The analysis was repeated for threshold values of .5, 1, 2, 4, and 8 meters. The results are generally intuitive:

- More extreme maneuvers are accompanied by longer periods of instability. Notably, though, the effect is not linear: for the 1-meter threshold, a 180° maneuver takes less than twice as long as a 45° maneuver, though it has 4 times the magnitude.

- Smaller maneuvers may not violate more permissive alignment criteria. For example, any maneuver smaller than 70° will not violate an 8-meter alignment threshold.

- Stricter alignment thresholds (such as .5 meters) may capture periodic misalignment outside of turns, leading to results that are less descriptive or repeatable.

While the results above are considered to hold under a range of AUVA geometries, the effect of absolute misalignment of elements on overall array performance can only be assessed in the context of the overall array and source geometry.

Cumulative Turn Effects

The path traced by the AUVA elements in each of the eight simulated missions is displayed in Figure 5-3, with the starting point circled in red. While the overall shape of each mission is apparent, departure from the edges is visible at the corners of the polygons. All polygonal missions progressed in a counter-clockwise direction. It can also be noted that the shapes appear slightly rotated; this is caused by the waypoint behavior of the lead element. Because all waypoints are slightly overshot, the lead element will tend to steady on a course to the right of the polygon edge, but slowly converging with it. However, since the determination of true target bearing depends on the *actual* lead element heading and not the ideal leg heading, this skew should not affect target localization (though array misalignment should).

44

(a) Picket (150 m)　　　(b) Picket (300 m)

(c) Triangle (200 m)　　(d) Square (150 m)　　(e) Pentagon (120 m)

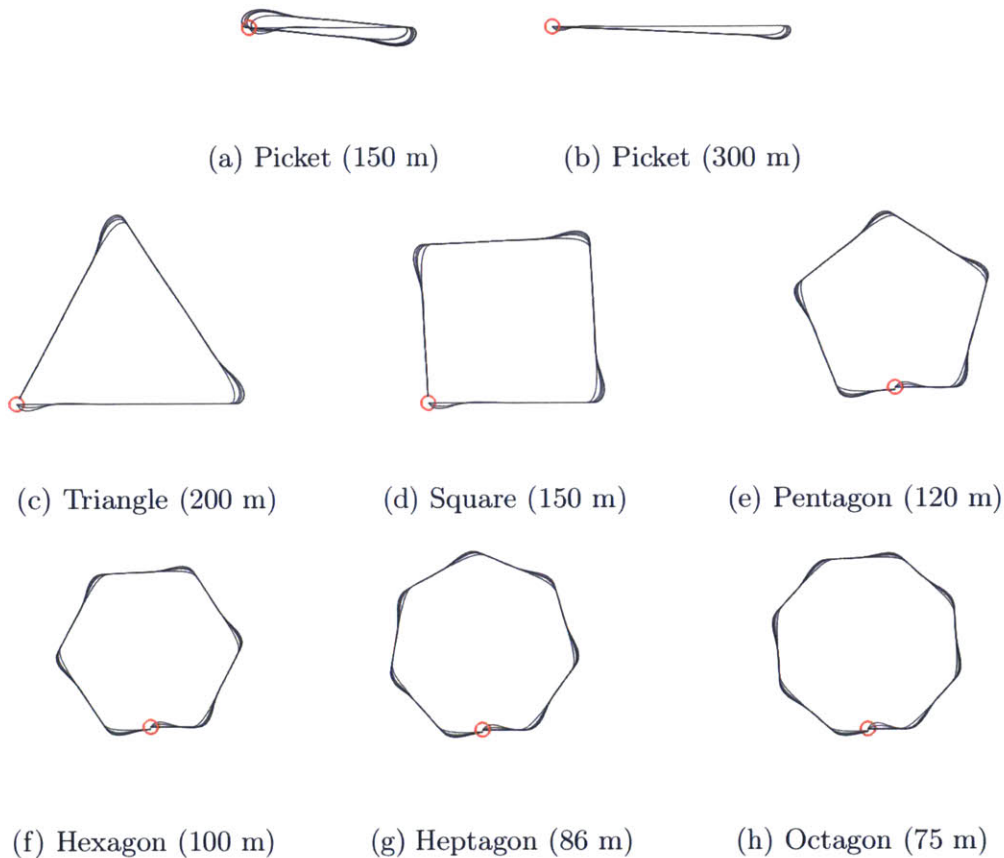(f) Hexagon (100 m)　　(g) Heptagon (86 m)　　(h) Octagon (75 m)

Figure 5-3: AUVA Element Paths (Edge Length)

Several factors simultaneously affect AUVA alignment throughout a mission. First, tighter (higher magnitude) turns are accompanied by longer periods of misalignment. For the constant perimeter, regular polygonal missions described here, however, tighter turns implies fewer turns and longer edge lengths; these two effects cancel each other to some effect. Smaller turns, which lead to small initial displacements, may also be accompanied by longer periods of slight misalignment as the elements slowly realign (Figure 5-1f through 5-1h).

Figure 5-4 describes the alignment performance of each mission over a range of alignment criteria. While the trend for each shape — more time aligned for more lenient criteria — is intuitive, the comparison between shapes is less so. The picket, triangle, and square missions are grouped with relatively high alignment, suggesting

that fewer turns and longer edge length are dominant in determining overall alignment. The pentagon, hexagon, and octagon shapes are almost never finely aligned. The alignment of the heptagon mission is particularly interesting: its fine alignment is better than that of both the hexagon and the pentagon, and its course alignment is the best of all the shapes.
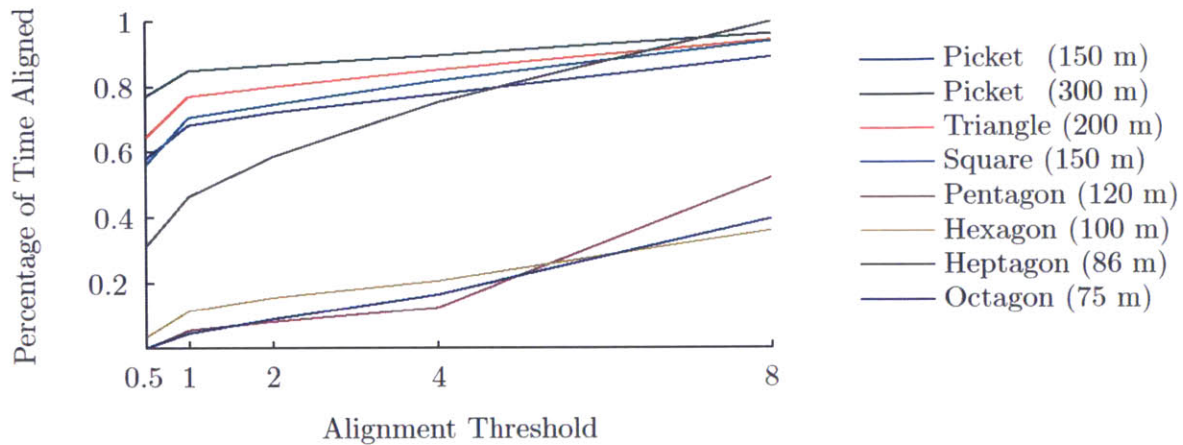

Figure 5-4: AUVA Alignment Percentage by Mission Shape

Alignment analysis of the missions supports two conclusions:

- Fewer turns and longer legs are the strongest predictors of array alignment over the course of a mission.

- Meaningfully predicting array misalignment would require more rigorous regression or factor analysis. In practice, however, the apparent sensitivity of alignment performance to various factors may favor direct simulation.

Array Scaling Effects

A single mission was simulated to test the effect of a larger array (more elements) on alignment performance. The triangle mission was modified to include nine vehicles, then run on the same course as before. Figure 5-5 summarizes the results. Notably, nearly doubling the number of elements had a relatively small effect on alignment performance — smaller, for example, than modifying the shape from a triangle to a square.
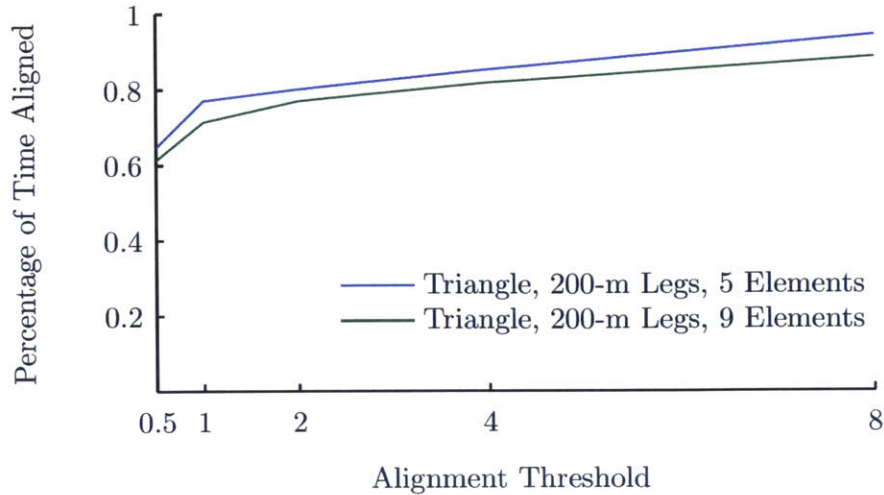
46

Figure 5-5: AUVA Mission Alignment Percentage by Number of Elements

5.2.2 Target Localization

For each of the time-series mission geometries previously described, *beamformer.m* (Section)4.3.4) provides a summary of the end-of-mission sonar response. The relative performance of the missions in this limited comparison is evident through visual inspection of Figures 5-6 through 5-8.

Target Scenario

As a basis of comparison, the source for each mission scenario was a 220-Hz narrowband source located on the x-axis at a range of 10,000 meters. At mission start, this corresponds to a target true bearing of 090°, although the true bearing changes slightly throughout the missions due to North-South excursion of the array.

It is expected that, holding other factors equal, changing the source location and characteristics would have some effect on the relative performance of the different missions. These differences are not expected to be great, however; analysis of a single target location is adequate to illustrate comparative performance for the purposes of this thesis.

47

Results

Figures 5-6 through 5-8 show the composite (average) array response, representing the cumulative source location information gathered by the AUVA over the duration of each mission.

The picket-shaped mission geometries are the simplest of the set from the standpoint of target motion analysis (TMA) in that, having only two unique legs on opposite courses, they do the least to resolve bearing ambiguity. Additionally, in this source scenario, the source is in the endfire region much of the time. Nothwithstanding, both missions result in a strong response region, approximately 90 degrees wide, centered on the true target location (Figures 5-6a and 5-6b). A secondary, but much smaller response region can be attributed to fore-aft ambiguity. Both figures indicate a positive bias in the estimated target location (black circle); this is attributed to the missions' consistent turns in one direction, as discussed in Section 5.2.1. The bias is more significant for the mission with 150-meter legs, as more time spent in maneuvers leads to a larger biased contribution to the average response.

The triangular mission represents the simplest approach to "complete" TMA in that it includes multiple, non-opposing legs while minimizing the number of maneuvers. Its simulated response (Figure 5-6c), in comparison to those of the picket missions, supports this. A single strong response region, approximately 45 degrees wide, is centered on the true target bearing. Multiple response regions are also visible on bearings of ambiguity, but due to the triangular geometry (each leg's heading is unique), none of these combine to become salient.

The square-shaped mission, with two sets of opposing legs, further illustrates the strengths of the triangular mission. In this case, the source location relative to the array track creates both fore-aft and left-right ambiguity, resulting in a strong secondary reponse on the opposite true bearing (Figure 5-7a). In addition, since the target is in the forward or aft endfire region of the array for two legs, both response regions are relatively wide. While the endfire phenomena is a product of the chosen source bearing, the replication of ambiguity regions is attributable to the mission
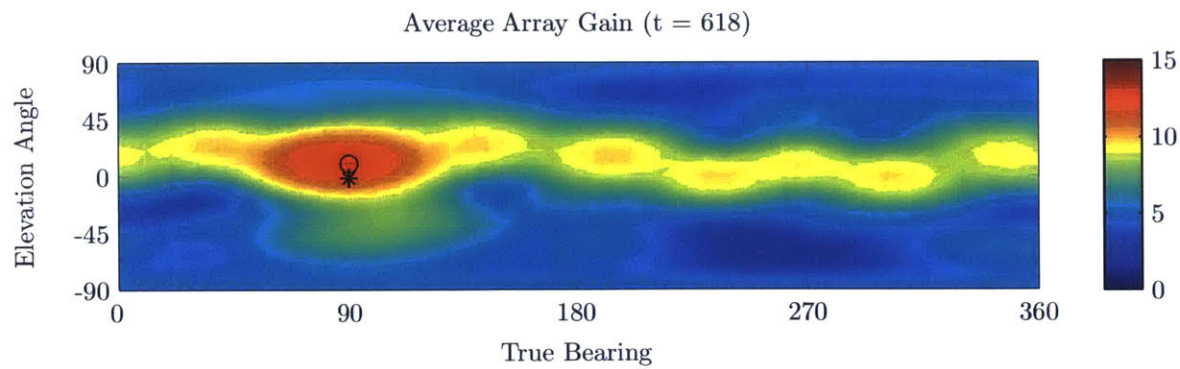
Average Array Gain (t = 628)

(a) Picket, 150-meter Legs

Average Array Gain (t = 620)
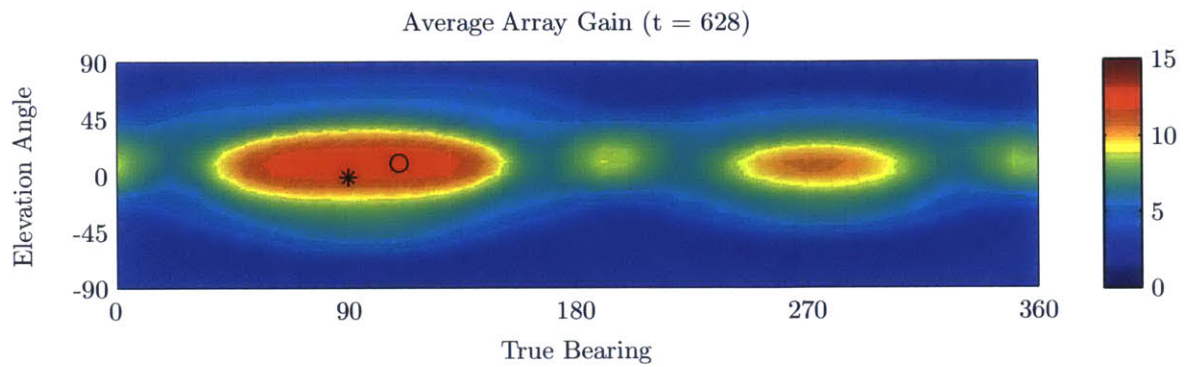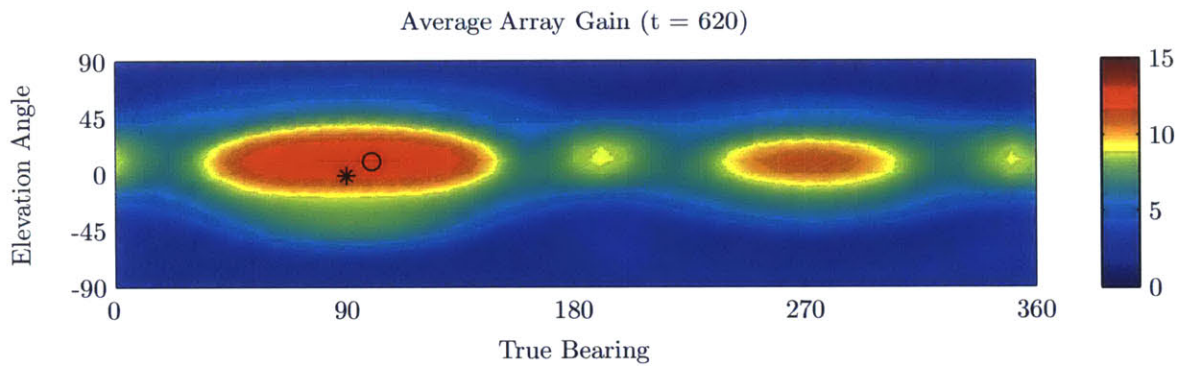
(b) Picket, 300-meter Legs

Average Array Gain (t = 618)

(c) Triangle, 200-meter Legs

Figure 5-6: Average (End-of-Mission) Array Response (1 of 3)

shape, regardless of source bearing.

The response of the remaining mission shapes (Figures 5-7b, 5-7c, and 5-8) are similar and illustrate the same general features:

- A single discernible region of strongest response, corresponding roughly to the true source bearing and elevation.

- One or more secondary response regions corresponding to the ambiguous bearing of each of the mission legs.

- An increasingly strong, level response at all bearings as the number of mission legs increases. This phenomenon is attributed to ambiguous bearing response as well as bias due to maneuvering.

- Similar to the above, a near-uniform increasing response at all bearings *and* elevations, attributed to misalignment of the vertical section during maneuvers.

Notably, in this scenario, the addition of mission legs over three does not improve localization performance; this supports the hypothesis that a triangular mission represents the most effective combination of multi-leg TMA and maneuver minimization.

Array Scaling Effects

As a continuation of Section 5.2.1, the sonar simulation was applied to a nine-element array running the triangular mission. The results (Figure 5-9) match those expected for an increase in array elements: finer bearing resolution results and smaller primary and secondary response areas. Two main secondary response areas are more salient, but the primary reponse is unambiguous. Importantly, there is no significant improvement in target localization.

Average Array Gain (t = 619)

(a) Square, 150-meter Legs

Average Array Gain (t = 630)
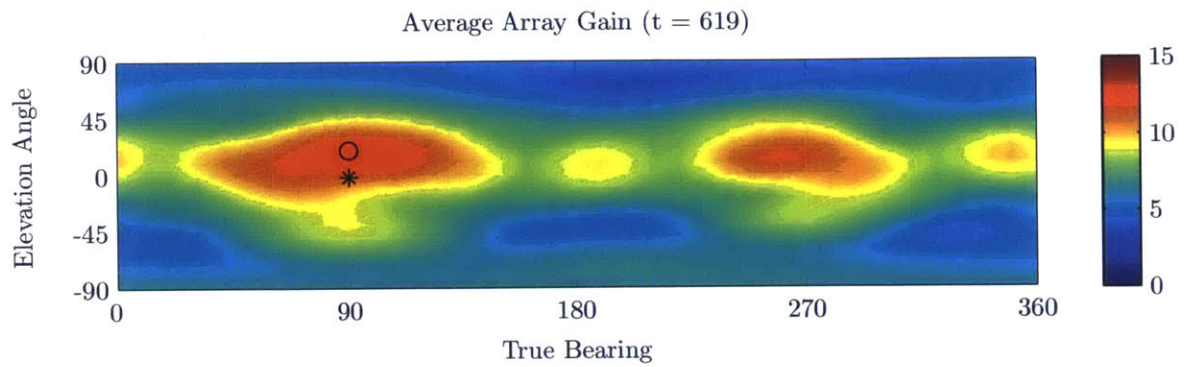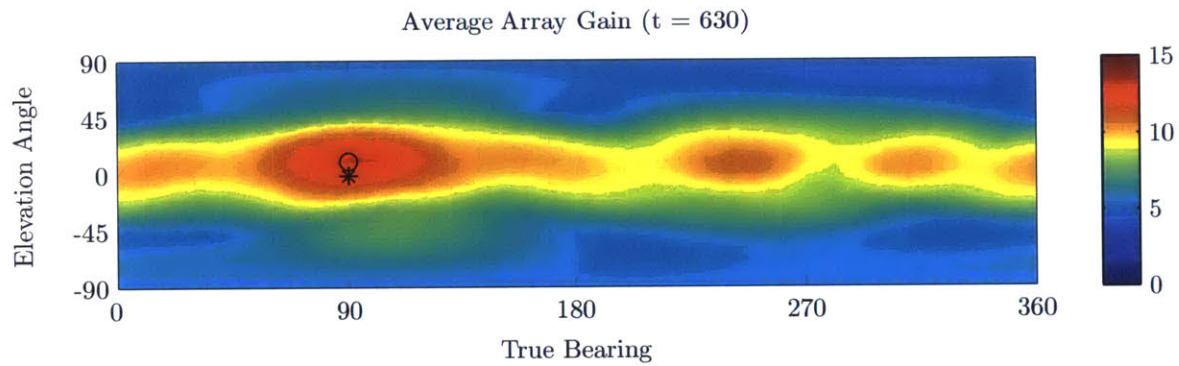
(b) Pentagon, 120-meter Legs

Average Array Gain (t = 622)
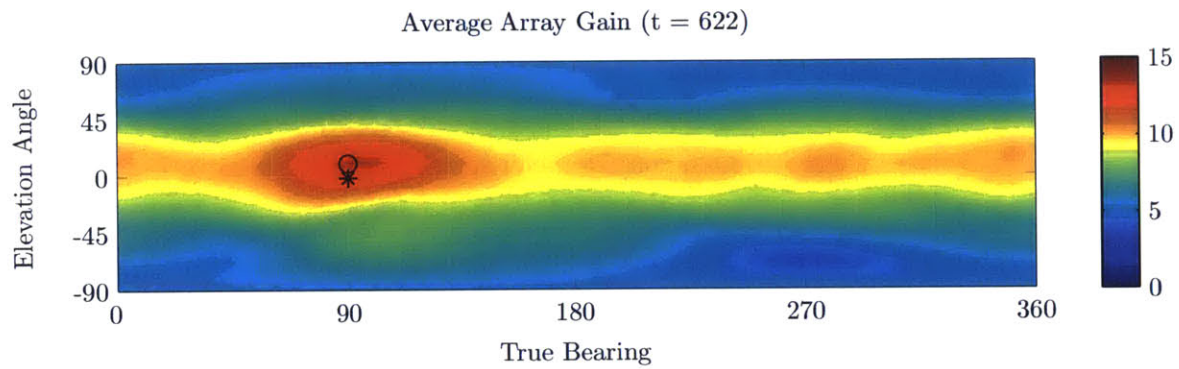
(c) Hexagon, 100-meter Legs

Figure 5-7: Average (End-of-Mission) Array Response (2 of 3)

Average Array Gain (t = 614)
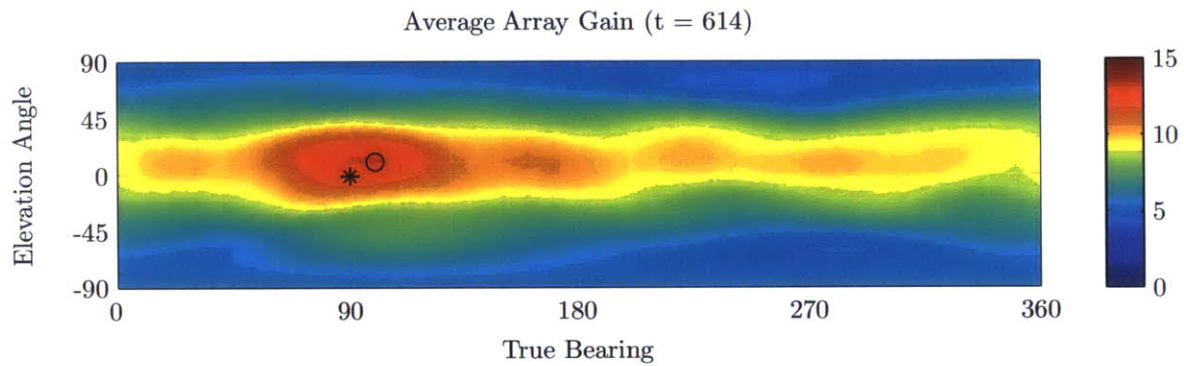
(a) Heptagon, 86-meter Legs

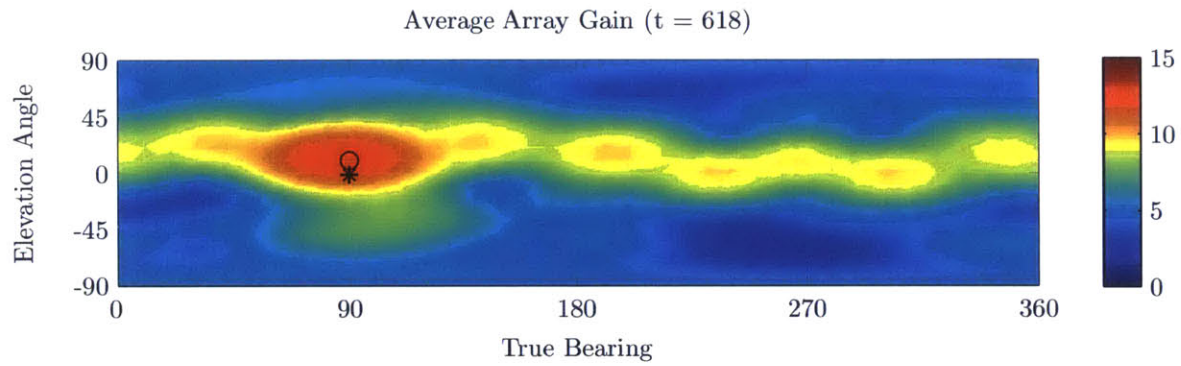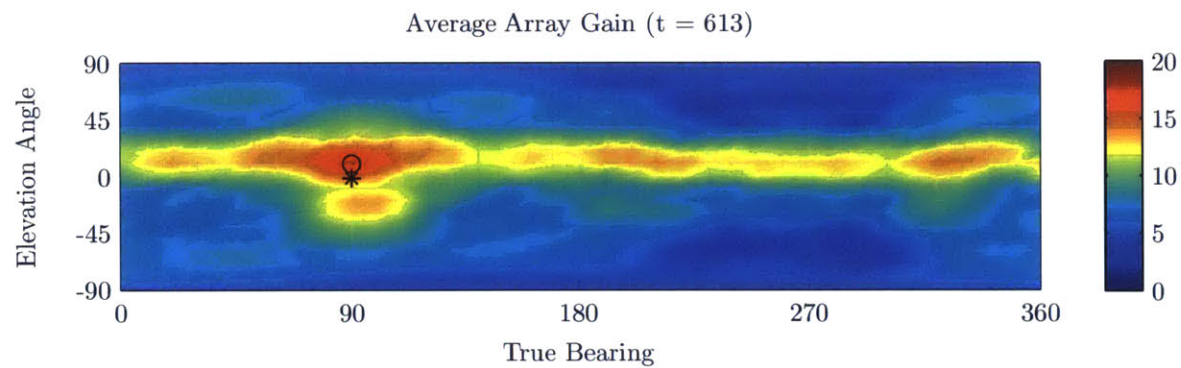Average Array Gain (t = 622)
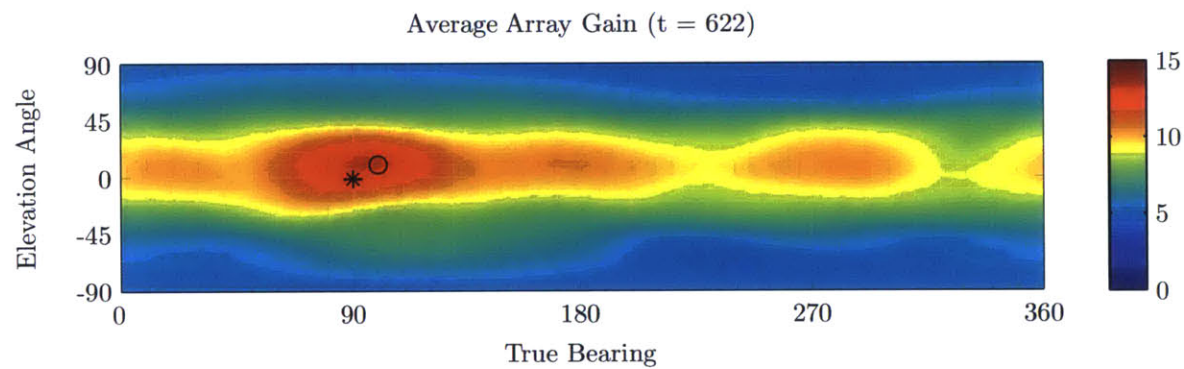
(b) Octagon, 75-meter Legs

Figure 5-8: Average (End-of-Mission) Array Response (3 of 3)

(a) Triangle, 200-meter Legs, 5 elements

(b) Triangle, 200-meter Legs, 9 elements

Figure 5-9: Comparison of Array Response for 5- and 9-element Arrays

53

THIS PAGE INTENTIONALLY LEFT BLANK

Chapter 6

Summary and Conclusions

6.1 General Methodology

The primary goal of this thesis was to evaluate, in simulation, a working example of an autonomous, multi-vehicle array. A secondary goal was to select tools, methods, and notional hardware in such a way that the evaluated array could be assembled, in the near future, with minimal modifications.

By virtue of programming in the MOOS-IvP environment, no modification to the basic array applications or behaviors — with the exception of inter-vehicle alignment, discussed below — would be necessary for the development of a physical prototype. Stock MOOS-IvP applications would, however, be required to interface with vehicle guidance and communication equipment.

As of writing, the *SandShark* AUV is in the final stages of development, to include at-sea measurement of performance parameters used in this simulation; the specific values chosen are considered to be approximate. It should be noted, however, that the AUVA behaviors are configurable and non-platform-specific; any number of vehicles may be incorporated into such an array. *SandShark* was chosen as an example based on its size, to facilitate optimal hydrophone spacing.

6.2 AUVA Performance

6.2.1 Alignment

The alignment behavior represented in this analysis by the *BHV_L_Element_Follow* code is an attempt at approximating the behavior of an inter-vehicle alignment system, and represents a departure from the software that would constitute a physical AUVA prototype. While it is expected that a real-time acoustic or optical alignment system would exhibit behaviors that are, in their specifics, different than what has been observed in simulation, the same general behaviors can be expected. Namely, delayed maneuvering response of non-lead elements leading to a period of instability and some degree of horizontal and/or vertical localization bias.

Alternatively, interpreted as a worst case, the alignment performance of the simulated AUVA is best judged by its effect on localization performance. No comparative analysis of alignment schemes is offered here.

6.2.2 Target Localization

Across all missions, a simple, narrowband beamformer applied to the time-series AUVA geometry resulted in a single discernable region of maximum response. In all cases, this region was centered approximately on the true location (bearing and elevation) of the target. This result validates the basic capability of an AUVA for acoustic target localization, and provides a basis for further development.

The relative localization performance of the missions suggests that in AUVA deployment planning, traditional TMA priorities — driving long legs on a maximum of unique bearings — can be effectively weighed against AUVA-specific concerns, such as mission time constraints and maneuvering cost, to produce a useful output.

6.3 Areas for Research

6.3.1 Generalized Performance

For practical reasons, the results of this analysis rely on several assumptions and parameter choices. Additionally, they reflect a single target scenario chosen for simplicity and commonality. The impacts of differing target scenarios are therefore not captured. The tools adopted by and developed for this research, however, could be readily applied to a more general analysis of AUVA performance across a wide variety of scenarios. This would be accomplished by modifying (for example): source location in three dimensions, AUVA geometry parameters, vehicle performance characteristics, or the acoustic environment.

6.3.2 Array Geometry

An L-shaped array was the focus of this research for the reasons outlined in Section 2.4, but may not be optimal for a variety of reasons, including theoretical acoustic performance or practical reasons yet to be identified. A meaningful exploration of the relative merits of different array shapes could be carried out entirely in simulation.

6.3.3 Broadband Processing

For simplicity, the scenario in this analysis was limited to a single narrowband source and rudimentary narrowband processing. A more sophisticated broadband processing scheme that more closely approximates real-world systems would produce results more easily evaluated against current capability.

More broadly, a physical prototype of an AUVA would ideally depart from purpose-built processing, and be designed to produce an acoustic output that is tailored to an existing processing software.

6.3.4 Multi-Element Vehicles

The primary benefit of distributing sensors over multiple vehicles is the ability to create a large aperture with a relatively small number of elements. This in no way precludes deployment of multiple sensors on each vehicle; this could only improve performance if processing capability is sufficient.

AUV-Towed Arrays

Numerous multi-sensor configurations are possible, including hull-mounted, towed, or a combination of these. A more complicated but flexible application of AUV-towed sensors would consist of hull-mounted sensors in combination with sensors towed at a variable distance, allowing for uniform (and adaptable) sensor spacing. As an alternative to adding vehicles, such a configuration may prove to leverage the AUVA concept while maximizing capability at minimal cost.

6.3.5 Adaptive Planning

For the AUVA concept presented here, adaptive planning requires the input of an operator, based on post-mission processing and interpretation. While the complete lack of in-situ data sharing between vehicles prohibits anything but the simplest adaptive planning, it is conceivable that one element (likely the lead element), if equipped with directional sensors, could be programmed to modify the mission in a predetermined way to optimize the result. This could include rotating or scaling the mission geometry in a way that is known to improve localization.

6.3.6 Inter-Vehicle Alignment

Satisfactory array alignment is fundamental to the feasibility of an AUVA. In this analysis, the behavior of a suitable inter-vehicle alignment system is approximated with *BHV_L_Element_Follow*, which requires an uncoded one-way data rate — the lead vehicle transmitting navigation data the other vehicles — of 20-30 bytes

per second. In a fully-functioning physical AUVA prototype, this behavior must be replaced by a true alignment system.

While data rates in excess of 30 bytes per second are not prohibitive for modern underwater modems, scaling such equipment to a relatively small vehicle may be difficult. Additionally, alignment based on broadcast of the lead element position requires that *all* elements know their three-dimensional position to an acceptable level of accuracy; the required systems in this case may prove prohibitive.

An alternative scheme is a real-time optical or acoustic system whereby each vehicle maintains relative alignment with the lead or an adjacent vehicle (rather than with datum). In each leader-follower pairing, the follower maintains relative alignment based on steady or periodic signals emitted by the lead.

6.3.7   Real-Time Data Sharing

The ability of AUVA elements to communicate during data collection has been excluded from this analysis as part of an effort to evaluate an AUVA design that is as simple as possible. Notwithstanding, underwater data transmission, though currently performance-limited, is a mature technology that could fundamentally change how the AUVA operates and performs. High-bandwidth optical and high-frequency acoustic systems are currently being explored.

A first application of data sharing between AUVA vehicles could be introduction of on-board processing. A simplified localization scheme — to the extent that processing power is limited — could provide the information necessary for a degree of adaptive planning.

As applied to inter-vehicle alignment, a data connection would allow direct sharing of lead vehicle coordinates. It is anticipated, however, that the utility of position sharing would be limited by two factors. First, bandwidth may be scarce if acoustic data is also shared; this would likely be a matter of choosing a balance that results in the desired performance. Second, even if the lead vehicle position is known, the limitations of AUV-deployed INS systems — which would be required in the absence of a relative positioning system — may place a limit on the best-case array alignment.

THIS PAGE INTENTIONALLY LEFT BLANK

Bibliography

[1] Arthur D. Anderson, III. *Cooperative autonomous tracking and prosecution of targets using range-only sensors.* c2013., 2013.

[2] A. B. Baggeroer, W. A. Kuperman, and Henrik Schmidt. Matched field processing: Source localization in correlated noise as an optimum parameter estimation problem. *Journal of the Acoustical Society of America*, 83(2):571, February 1988.

[3] Michael R. Benjamin, Henrik Schmidt, Paul Newman, and John J. Leonard. *An Overview of MOOS-IvP and a users guide to the IvP Helm, release 4.2.1.* Technical report: MITSG 11-29. Cambridge, Mass. : Sea Grant College Program, Massachusetts Institute of Technology, [2011]., 2011.

[4] Deanna M. Caveny, Donald R. Del Balzo, James H. Leclere, and George E. Ioup. Performance of sinusoidally deformed hydrophone line arrays. *Journal of the Acoustical Society of America*, 105(4):2203, April 1999.

[5] B. Fletcher. UUV master plan: a vision for navy UUV development. In *OCEANS 2000 MTS/IEEE Conference and Exhibition*, volume 1, pages 65–71 vol.1, 2000.

[6] Katerina Kaouri. *Left-Right Ambiguity Resolution of a Towed Array Sonar.* PhD thesis, Univeristy of Oxford, 2000.

[7] Jonathan Paul Kitchens. *Acoustic vector-sensor array processing.* PhD thesis, c2010., 2010.

[8] Wa Kuperman and Dr Jackson. Ocean acoustics, matched-field processing and phase conjugation. In *IMAGING OF COMPLEX MEDIA WITH ACOUSTIC AND SEISMIC WAVES*, volume 84, pages 43–96. 2002.

[9] M. Lasky, R.D. Doolittle, B.D. Simmons, and S.G. Lemon. Recent progress in towed hydrophone array research. *IEEE Journal of Oceanic Engineering*, 29(2):374–387, April 2004.

[10] S.G. Lemon. Towed-array history, 1917-2003. *IEEE Journal of Oceanic Engineering*, 29(2):365–373, April 2004.

[11] Qihu Li. *Digital Sonar Design in Underwater Acoustics: Principles and Applications*. Springer Science & Business Media, March 2012.

[12] D. Mauuary, B. Faure, and A. Essebarr. Vertical synthetic aperture sonar for ocean acoustic tomography. *IEEE Journal of Oceanic Engineering*, 23(1):47–59, January 1998.

[13] Michael B. Porter. Test, January 2011.

[14] William I. Roderick and William A. Von Winkle. Expendable virtual vertical sensing array, August 1991. U.S. Classification 367/119, 367/3, 367/124; International Classification G01S11/14; Cooperative Classification G01S11/14; European Classification G01S11/14.

[15] Robert E. Sheriff and L. P. Geldart. *Exploration seismology*. Cambridge ; New York : Cambridge University Press, 1994., 1994.

[16] Unknown. Solid streamers demonstrating better operations up-time. *Offshore Magazine*, 60(4), April 2000.

[17] US Navy. Final Comprehensive Report for the Operation of the Surveillance Towed Array Sensor System, January 2007.

[18] M. Žuvić. The Story of the Liberty Ships. *Transactions on Maritime Science*, 2(2):133–142, November 2013.